

The effect of solvation on molecular Rydberg states: Dioxane clustered with nonpolar solvents

P. O. Moreno, Q. Y. Shang, and E. R. Bernstein

Citation: *The Journal of Chemical Physics* **97**, 2869 (1992); doi: 10.1063/1.463029

View online: <http://dx.doi.org/10.1063/1.463029>

View Table of Contents: <http://aip.scitation.org/toc/jcp/97/5>

Published by the *American Institute of Physics*

COMPLETELY

REDESIGNED!



**PHYSICS
TODAY**

Physics Today Buyer's Guide
Search with a purpose.

The effect of solvation on molecular Rydberg states: Dioxane clustered with nonpolar solvents

P. O. Moreno, Q. Y. Shang, and E. R. Bernstein
Colorado State University, Chemistry Department, Fort Collins, Colorado 80523

(Received 30 March 1992; accepted 22 May 1992)

One color $2+1$ mass resolved excitation spectroscopy is employed to obtain molecular Rydberg $3s \leftarrow n$ transition spectra of 1,4-dioxane clustered in a molecular beam with nine nonpolar solvents. The solvents are Ar, Kr, CH₄, CD₄, CF₄, SiH₄, Si(CH₃)₄, ethane, *n*-propane, cyclohexane-*h*₁₂, and cyclohexane-*d*₁₂. Spectral results are interpreted in terms of cluster size, isotope effects, and model calculations. A Lennard-Jones-Coulomb 6-12-1 potential is used to model the intermolecular interactions and predict minimum energy cluster geometries, cluster binding energies, and intermolecular force constants which are used to calculate van der Waals vibrational frequencies. The results show that for simple solvents (i.e., Ar, CH₄) the calculations offer a simple interpretation of the observed spectra in terms of multiple cluster geometries with distinct transition energies; however, as the solvent becomes more complex, the cluster spectra also become more complex, and the number of calculated minimum energy cluster geometries increases. Complex spectra are interpreted as a distribution of cluster geometries with similar transition energies. For all of the clusters, the electronic origins are blue shifted with respect to the bare 1,4-dioxane origin. This observation is consistent with a model in which the excited state intermolecular potential becomes more repulsive due to the increased radial distribution of a nonbonding electron upon excitation into the 3s Rydberg state.

I. INTRODUCTION

The main body of molecular electronic spectroscopic information for organic systems concerns valence ($n \rightarrow \pi^*$) or ($\pi \rightarrow \pi^*$) transitions. These transitions promote an electron into an antibonding orbital (within the $n=2$ atomic shell) and the resulting spectra, therefore, reflect the structure of a state with antibonding character. Thus, these studies are necessarily limited to systems which possess a π -bond moiety. Alternatively, molecular Rydberg spectroscopy involves the promotion of a nonbonded, lone-pair, σ -bond, or π -bond electron to a nonbonding orbital of higher principle quantum number (e.g., $n=3$). Since all molecules possess such electrons, this dramatically expands (i) the range of systems which can be studied at high resolution and sensitivity, and (ii) the type of information available for molecules. A body of information concerning Rydberg transitions in bare molecules exists.¹ The current collection of Rydberg data, however, is deficient in a number of ways: (i) it has been mostly acquired by one photon excitation, (ii) the systems studied are generally rotationally and vibrationally hot, resulting in highly congested spectra, and (iii) the detection techniques used do not employ mass spectroscopy, and therefore do not provide for discrimination against impurities. Molecular beam/laser spectroscopy addresses these limitations. Baer *et al.* have recently studied Rydberg transitions in a number of jet cooled cyclic ketones and methyl substituted cyclic ketones.² The resulting spectra are characterized by low vibrational and rotational temperatures, very narrow peaks, and high signal-to-noise ratios. The information contained in these well resolved vibronic molecular Rydberg spectra can be used for the characterization of slight changes in ring structure, and the position and orientation

of substituents. Of particular interest to this work is the observation of the two photon ($n \rightarrow 3s$) transition in 1,4-dioxane.³ Also, Grant *et al.* have studied Rydberg states of jet cooled benzene,⁴ toluene,⁵ *sym*-triazine,⁶ and cyclohexane.⁷

The development of molecular jet technology has elicited a great deal of interest in the identification and spectroscopy of molecular clusters.⁸ Such studies are vital to the understanding of solvation effects since the clustered molecule represents a bridge between the extreme cases of isolated, gas phase molecules and condensed phase totally solvated molecules.

Presently, the majority of the electronic spectroscopic studies of clusters are of complexes of organic species, specifically aromatic molecules. These studies⁸ focus on (i) the direction and extent of the transition energy perturbation upon clustering, (ii) modeling the most stable cluster geometries, (iii) normal mode analysis and assignment of van der Waals (vdW) vibrational modes, (iv) modeling the intermolecular binding energies, (v) cluster vibrational dynamics and dissociation, and (vi) cluster chemistry. Due to their spatially extended orbitals, Rydberg excitations should be very sensitive to solvation effects and cluster chemistry. Indeed, one of the main experimental methods for distinguishing Rydberg transitions from valence transitions has been the relative amount of spectral broadening induced by an applied bath gas pressure.¹ To date, virtually no information concerning the specific effects of clustering on molecular Rydberg transitions exists. Vaida *et al.* have provided evidence for cluster induced perturbation of the Rydberg spectra of acetone,⁹ acetaldehyde,¹⁰ and methyl iodide.¹¹ In those experiments the amount of

transmitted vs absorbed light is measured, but species (i.e., monomer, dimer, trimer, etc.) are not determined.

In this paper, we report the first mass resolved Rydberg spectra of jet cooled clusters. The solute, 1,4-dioxane, is clustered in a molecular beam with various solvents including Ar, Kr, CH₄, CD₄, CF₄, SiH₄, Si(CH₃)₄, ethane, *n*-propane, cyclohexane-*h*₁₂, and cyclohexane-*d*₁₂. Spectra are acquired via a one color, resonance enhanced, (2+1) mass resolved excitation spectroscopy (MRES).¹² This technique offers five important advantages with regard to previous studies of bare molecule Rydberg transitions. First, two photon selection rules allow access to electronic states which are not allowed via a one photon transition. Second, it makes high energy (less than 200 nm) electronic states accessible with visible or UV laser radiation. Third, valence transitions in this regime are usually broad due to high state densities and short lifetimes: molecular Rydberg states, on the other hand, are decoupled from valence states and are relatively long lived and sharp. The result is that Rydberg spectra appear as sharp lines built on the broad background of higher valence transitions.¹ Fourth, molecular Rydberg states typically have large ionization cross sections which facilitate their discrimination from valence transitions and generate intense spectra. Fifth, resolution facilitates the identification of observed species and avoids the possibility of overlapping and interfering cluster spectra.

In the following discussion, the results of the present work are interpreted in terms of cluster size (mass), isotope effects, and predictions based on some simple model calculations. Similar techniques have previously proven useful in the analysis of valence transition spectroscopic data for molecular clusters.⁸ Model calculations provide three types of information which facilitate the analysis of the experimental spectra. First, the minimum energy cluster geometries are determined with an empirical intermolecular potential. Second, the calculations also provide binding energies for the various geometries. And finally, a normal mode analysis of the cluster vibrations is performed for the determined cluster geometries to predict van der Waals vibrational frequencies and compare them with experimental observations.

II. PROCEDURES

A. Experiment

A detailed description of the supersonic molecular jet apparatus and time-of-flight mass spectrometer has been published previously.¹³ Light from a Nd/YAG pumped dye laser (Spectra Physics) is mixed with the Nd/YAG 1.064 μm fundamental to produce a UV/VIS excitation beam. A 2:1 DCM/R640 (Exiton) laser dye mixture in methanol is used to span the range of wavelengths (383–405 nm) required for these studies. A 35 cm focal length lens is used to focus the resulting laser beam onto the molecular beam. MRES spectra are acquired by employing a pulsed supersonic molecular jet expansion in combination with one color 2+1 resonance enhanced ionization. Following ionization, the molecular and cluster ions are

subsequently analyzed by time-of-flight mass spectroscopy. Nozzle backing pressure is maintained at 50 psi (gauge). Samples of gas mixtures consisting of 1% solute (1,4-dioxane) and 5% solvent (i.e., methane, etc.), with a balance of bath gas (helium), are prepared in the following manner. First, a stainless steel vacuum manifold and mixing tank are evacuated to ca. 10⁻³ Torr. The solute is then degassed and an appropriate amount (ca. 50 Torr) is introduced to the system. The solvent is then introduced in the appropriate amount, and the bath gas subsequently added. This sequence is adopted so that the mixing vessel is kept at a lower total pressure than the substance being introduced. The sources and purities of materials used are as follows: 1,4-dioxane (Mallinckrodt, AR), argon (General Air, Commercial Grade), krypton (Spectra Gases, 99.995%), methane-*h*₄ (General Air, Commercial Grade), methane-*d*₄ (Cambridge Isotope Laboratory, 99%), ethane (Matheson, Research Grade), propane (Scientific Gas Products, Research Grade), cyclohexane-*h*₁₂ (Fisher, Spectrograde), cyclohexane-*d*₁₂ (Aldrich, 99.5%), silane (Aldrich, 99.9%), tetramethylsilane (Aldrich, NMR Grade), tetrafluoromethane (Aldrich, 912%). All reagents are used without additional purification.

B. Calculation

Three types of calculations are performed to model the studied clusters. First, the ground state minimum energy cluster geometries are determined using three different empirical potential energy methods. Second, the 1,4-dioxane(CH₄)₁ cluster geometry is modeled with a semiempirical molecular orbital method. Third, a normal mode analysis is performed with these geometries to determine cluster van der Waals vibrational frequencies.

The ground state minimum energy cluster geometries for the 1,4-dioxane(CH₄)₁ are determined using four different methods. First, the potential parameters and methods of Scheraga are used with fixed solvent and solute geometries.¹⁴ These calculations employ as many as 2000 random starting points with a Lennard-Jones–Coulomb 6-12-1 potential. The solvent and solute geometries and atomic partial charges are determined by a semiempirical molecular orbital calculation with the computer program MOPAC 6,¹⁵ employing the PM3 Hamiltonian. Second, the WERK force field of Rappé *et al.*¹⁶ is used to calculate cluster geometries while allowing the solute and solvent molecular geometries to relax as a result of the intermolecular potential energy. Partial charges used in this calculation are the same as those used for the previous method. This algorithm also uses a Lennard-Jones–Coulomb 6-12-1 expression for modeling van der Waals interactions. Third, the MMX force field of Gajewski and Gilbert, which is an extension of Allinger's MM2 force field,¹⁷ is employed to calculate the cluster geometries while allowing the solute and solvent molecular geometries to relax. Methods 2 and 3 use only a limited number of input geometries which are chosen to be close to the minimum energy geometries determined by method 1 above. Fourth, these minimum energy geometries for the 1,4-dioxane(methane)₁ cluster also serve as starting geometries for the semiempirical molecu-

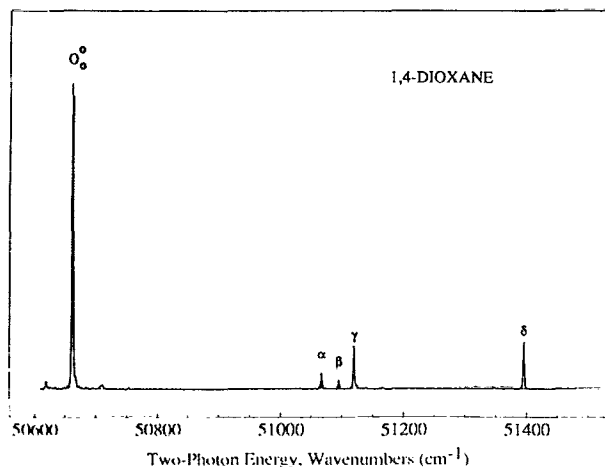


FIG. 1. Two photon one color (2+1) mass resolved excitation spectrum (MRES) of 1,4-dioxane. The electronic origin (0_0^0) is at $50\,663.1\text{ cm}^{-1}$ and the peaks labeled α, β, γ , and δ are dioxane excited state internal vibrations. The small peaks on both sides of the origin are hot bands.

lar orbital package MOPAC 6. MOPAC 6 calculations employ the PM3 Hamiltonian with the gradient norm reduced to 10^{-3} . Calculations for all other clusters are restricted to method 1.

A normal mode analysis is performed on the minimum energy cluster geometries resulting from method 1 and the van der Waals vibrational frequencies are determined. This type of calculation is described in detail elsewhere.¹⁸ Translational and rotational degrees of freedom have residual energies of less than 10^{-2} cm^{-1} for all normal mode calculations.

III. RESULTS AND DISCUSSION

Figure 1 presents the mass resolved excitation spectrum MRES (2+1) of the bare 1,4-dioxane molecule. This spectrum is similar to that reported by Ref. 3. The transition energy for the electronic origin (0_0^0 transitions) of 1,4-dioxane is $50\,663.1\text{ cm}^{-1}$. This is the lowest energy electronic transition observed in 1,4-dioxane and it is only observed in two-photon absorption. It is assigned as an $n\text{-}3s$ Rydberg transition: $2A_g \leftarrow 1A_g, 3s \leftarrow n$, two photon allowed, one photon forbidden. The first four vibronic transition appears at $51\,067.9\text{ cm}^{-1}$ (labeled α), $51\,096.5\text{ cm}^{-1}$ (labeled β), $51\,120.7\text{ cm}^{-1}$ (labeled γ), and $51\,396.9\text{ cm}^{-1}$ (labeled δ) corresponding to 404.8 cm^{-1} , 433.4 cm^{-1} , 457.6 cm^{-1} , and 733.8 cm^{-1} excited state vibrations, respectively. The two photon energies for the vibronic features of 1,4-dioxane are listed in Table I, both as absolute energies, and as energies relative to the 1,4-dioxane origin. In presenting and discussing the subsequent cluster data, this spectrum will serve as a comparison for shifts and changes in vibrational frequencies.

A. Dioxane(Kr)₁ and (Ar)₁

The middle trace in Fig. 2 is the MRES of 1,4-dioxane(Kr)₁ cluster. Notice that the bare dioxane transitions can be seen in the cluster spectrum as negative

peaks due to overload ringing from the nearby solute mass channel. The origin of the cluster spectrum (labeled A) at $50\,685.7\text{ cm}^{-1}$ is blue shifted 22.6 cm^{-1} with respect to the bare dioxane origin and a second feature (labeled B) at $50\,770.0\text{ cm}^{-1}$ is blue shifted by 106.7 cm^{-1} . Built on each of these transitions is a set of three features which correspond to dioxane vibronic transitions, labeled $A_{\alpha}, A_{\beta}, A_{\gamma}$ and $B_{\alpha}, B_{\beta}, B_{\gamma}$. A_{α} and B_{α} are 411 cm^{-1} from A and B, respectively. Transition B at $50\,770.0\text{ cm}^{-1}$ may be assigned in two ways: (i) as the electronic origin of a second stable cluster geometry, or (ii) as an intermolecular van der Waals vibrational mode built on A. In either case, the features built on it, B_{α}, B_{β} , and B_{γ} may be assigned as internal 1,4-dioxane vibronic transitions.

The top trace in Fig. 2 is the MRES of 1,4-dioxane(Ar)₁ cluster. This spectrum is very similar to that of the 1,4-dioxane(Kr)₁ cluster. The origin of the 1,4-dioxane(Ar)₁ spectrum at $50\,723.5\text{ cm}^{-1}$ (labeled A) is blue shifted by 60.4 cm^{-1} relative to the 1,4-dioxane origin and the second feature at $50\,821.7\text{ cm}^{-1}$ (labeled B) appears blue shifted by 158.6 cm^{-1} . While the three dioxane vibronic peaks (labeled A_{α}, A_{β} , and A_{γ}) built on cluster origin A are present in the 1,4-dioxane(Ar)₁ spectrum, only one vibronic feature in the second group built on B (labeled B_{α}) is visible above the noise level.

Typically for valence transitions, argon and krypton clusters have red shifted transitions with respect to the bare molecule spectrum and additionally, the cluster shift is larger for krypton than for argon. The reverse is seen here for the Rydberg transition: this indicates that the $3s$ Rydberg state cluster is more weakly bound than the ground state cluster.

Two minimum energy geometries are calculated for the 1,4-dioxane(Ar)₁ cluster by method 1 described in Sec. II B. In order to describe these calculated geometries, the orientation of the solute molecule is defined in the following manner. First, consider a coordinate system for which the origin is at the center of a rectangle defined by the four carbon atoms of dioxane. The z axis is perpendicular to the plane of the dioxane carbon atoms, the x axis is normal to the C-C bonds, and the y axis necessarily lies in the vertical C_2 plane containing the oxygen atoms. In the most stable of the two geometries, the argon atom lies along the z axis and, in the second geometry, the argon atom lies in the y, z plane slightly above the y axis. These minimum energy configurations along with their respective binding energies (BE) are presented in Fig. 3. The argon atom lies along the z axis for the lowest energy cluster geometry. A normal mode analysis is performed on these cluster geometries to determine the intermolecular van der Waals vibrational frequencies and these are listed in Table II for both cluster geometries.

The spectral shift for a cluster may be seen as the difference between the ground and excited state binding energies. A blue shift implies the destabilization of the cluster upon excitation to its molecular Rydberg state. For both the 1,4-dioxane(Ar)₁ cluster and the 1,4-dioxane(Kr)₁ cluster, no signal is observed above $51\,250\text{ cm}^{-1}$: this is 527 cm^{-1} and 564 cm^{-1} higher in

TABLE I. Transition energies and assignments for various solvents clustered with 1,4-dioxane.^a

Species	Label	Transition energies (cm ⁻¹)	Relative energies (cm ⁻¹)		Assignment
			Origin	Vibrations	
1,4-dioxane	O_0^0	50 663.1	0.0		1,4-dioxane origin
	α	51 067.9		404.8	IV
	β	51 096.5		433.4	IV
	γ	51 120.7		457.6	IV
	δ	51 396.9		733.8	IV
Solvent: Krypton	A	50 685.7	22.6		Cluster origin
	A_α	51 096.3		410.6	IV
	A_β	51 125.1		439.4	IV
	A_γ	51 143.5		457.8	IV
	B	50 770.0	106.7		Cluster origin
	B_α	51 181.3		411.3	IV
	B_β	51 211.6		441.6	IV
	B_γ	51 228.2		458.2	IV
Argon	A	50 723.5	60.4		Cluster origin
	A_α	51 113.5		390.0	IV
	A_β	51 161.6		438.1	IV
	A_γ	51 181.0		457.5	IV
	B	50 821.7	158.6		Cluster origin
	B_α	51 231.4		409.7	I.V.
CH ₄	A	50 673.5	10.4		Cluster origin
		50 676.9		3.4	vdW
		50 679.1		5.6	vdW
		50 681.9		8.4	vdW
	a_1	50 737.6		64.1	vdW
	B	50 792.8	129.7		Cluster origin
		50 795.8		3.0	vdW
		50 798.7		5.9	vdW
CD ₄	C	50 851.4	188.3		Cluster origin
	A	50 676.2	13.1		Cluster origin
	a	50 677.8		1.6	vdW
	50 727.1		50.9	vdW	
	B	50 797.9	134.8		Cluster origin
		50 799.2		1.3	vdW
CF ₄	C	50 851.4	188.3		Cluster origin
	A	50 979.3	316.2		Cluster origin
	a_1	51 008.5		29.2	vdW
	A_α	51 390.3		411.0	IV
	B	51 070.0	406.9		Cluster origin
	b_1	51 074.9		4.9	vdW
	b_2	51 077.9		7.9	vdW
	B_α	51 485.3		415.3	IV
	B_β	51 508.9		438.9	IV
	B_γ	51 528.4		458.4	IV
	$b_{1\alpha}$	51 490.3		5.0	vdW
	$b_{2\alpha}$	51 494.9		9.6	vdW
	C	51 093.6	430.5		Cluster origin
	Ethane	A	50 717.1	54.0	
a_1		50 720.9		3.8	vdW
a_2		50 735.4		18.3	vdW
a_3		50 746.7		29.6	vdW
A_α		51 127.8		410.7	IV
A_β		51 157.9		440.8	IV
A_γ		51 175.1		458.0	IV
A_δ		51 446.9		729.8	IV
B		50 851.4	188.3		Cluster origin

TABLE I. (Continued.)

Species	Label	Transition energies (cm ⁻¹)	Relative energies (cm ⁻¹)			
			Origin	Vibrations	Assignment	
Propane	<i>b</i> ₁	50 889.0		37.6	vdW	
	<i>C</i>	50 907	244		Cluster origin	
	<i>C</i> _α	51 324		417	IV	
	<i>A</i>	50 756.4	93.3		Cluster origin	
	<i>a</i> ₁	50 781.0		24.6	vdW	
	<i>a</i> ₂	50 805.2		48.8	vdW	
	<i>A</i> _α	51 165.9		409.5	IV	
	<i>A</i> _β	51 195.2		438.8	IV	
	<i>A</i> _γ	51 213.5		457.1	IV	
	<i>B, C</i>	50 988.8	325.7		Cluster origin	
	51 004.0	340.9		Cluster origin		
	[<i>B, C</i>] _α	51 404.5		415.7	IV	
		51 417.6		413.6	IV	
C ₆ H ₁₂	<i>A</i>	50 811.1	148.0		Cluster origin	
	<i>A</i> _α	51 225.8		414.7	IV	
	<i>A</i> _δ	51 548.2		737.1	IV	
	[<i>B, C</i>]	50 839.7	176.6		Cluster origin	
		50 856.6	193.5		Cluster origin	
	[<i>B, C</i>] _α	51 253.5		413.8	IV	
		51 269.6		413.0	IV	
	[<i>B, C</i>] _δ	51 574.0		734.3	IV	
		51 595.5		738.9	IV	
	C ₆ D ₁₂	<i>A</i>	50 820.8	157.7		Cluster origin
<i>A</i> _α		51 235.9		415.1	IV	
<i>A</i> _δ		51 558.1		737.3	IV	
[<i>B, C</i>]		50 848.8	185.7		Cluster origin	
		50 871.0	207.9		Cluster origin	
[<i>B, C</i>] _α		51 260.8		412.0	IV	
		51 279.0		408.0	IV	
[<i>B, C</i>] _δ		51 584.5		735.7	IV	
		51 607.2		736.2	IV	
SiH ₄		<i>A</i>	50 999.9	336.8		Cluster origin
	<i>a</i> ₁	51 014.8		14.9	vdW	
	<i>A</i> _α	51 416.4		416.5	IV	
	<i>A</i> _δ	51 732.3		732.3	IV	
	<i>B</i>	51 033.6	370.5		Cluster origin	
		51 036.4	373.3		Cluster origin	
		51 040.9	377.8		Cluster origin	
	<i>B</i> _α	51 452.0		418.4	IV	
	<i>B</i> _γ	51 769.0		735.4	IV	
	<i>C</i>	51 075	412			
	TMS	[<i>A, B, C</i>]	51 138	475		Cluster origin
		[<i>A, B, C</i>] _{αβγ}	51 548		410	IV
		[<i>A, B, C</i>] _γ	51 868		730	IV

*IV denotes solute internal vibrational modes, while vdW denotes intermolecular van der Waals modes.

energy than the low energy cluster spectral origin for the 1,4-dioxane(Ar)₁ and 1,4-dioxane(Kr)₁ clusters, respectively. The clusters must be dissociating due to intracuster vibrational energy redistribution (IVR) of excess vibrational energy and subsequent vibrational predissociation (VP). This cluster dissociation is additionally confirmed by the observation of the cluster features in the bare molecule mass channel. The vibrational excess energy at which cluster signals are no longer observed represents an upper

bound on the excited state cluster binding energy. An upper bound for the ground state binding energy may then be determined by adding the spectral shift to these numbers. The experimentally determined upper limit for the ground state binding energies of the 1,4-dioxane(Ar)₁ and 1,4-dioxane(Kr)₁ clusters are larger than the calculated ground state binding energies as expected since IVR might well be slow in this system.

The peaks labeled A and B in the 1,4-dioxane(Ar)₁

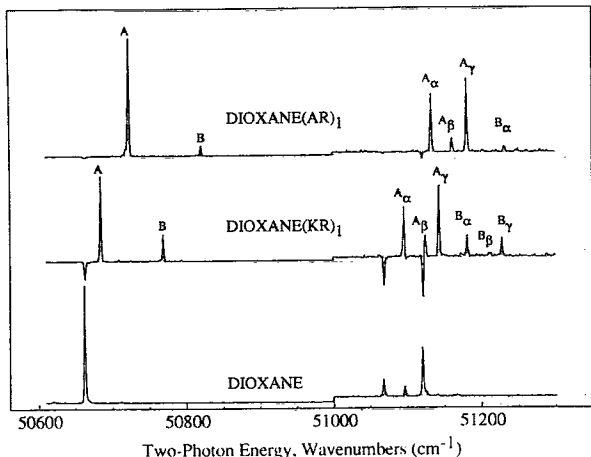


FIG. 2. Two photon one color (2+1) MRES of 1,4-dioxane (bottom trace), 1,4-dioxane(Kr)₁ cluster (center trace), and 1,4-dioxane(Ar)₁ cluster (top trace). For energies above 51 000 cm⁻¹, intensities have been increased by a factor of 5.

spectrum are assigned as the spectral origins (0_0^0 transitions) for two cluster configurations. This assignment is based on: (i) the cluster minimum energy calculations which predict two stable configurations for this cluster, and (ii) the normal mode analysis of these configurations which predicts that the highest van der Waals vibrational frequency is 36 cm⁻¹ for either cluster geometry. This is only about 40% of the 98 cm⁻¹ difference between the two features labeled A and B and suggests that B is not due to a van der Waals vibration because all the intensity for the cluster transition is at the 0_0^0 transition. Hence, the observed spectrum consists of two overlapping spectra resulting from the two stable cluster geometries. The features

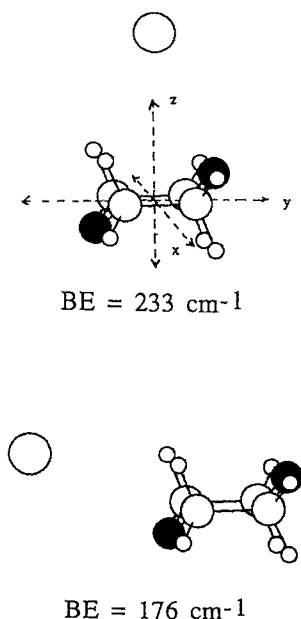


FIG. 3. The two minimum energy configurations and their binding energies for the 1,4-dioxane(Ar)₁ cluster simulated with Scheraga's potential.

TABLE II. van der Waals normal mode frequencies (cm⁻¹) and mode types for two 1,4-dioxane(Ar)₁ cluster geometries.^a

Cluster binding energy 233 cm ⁻¹	Mode type ^b	Cluster binding energy 176 cm ⁻¹	Mode type
35.6	<i>S_x</i>	32.3	<i>S_y</i>
27.6	<i>B_y</i>	19.8	<i>B_x</i>
23.6	<i>B_x</i>	14.4	<i>B_z</i>

^aFigure 3 illustrates the geometries of the two 1,4-dioxane(Ar)₁ geometries and the defined x, y, and z axis.

^bMode types stretch (S) and bend (B) have been defined in Ref. 21. The direction of motion indicated by the subscripts is approximate since the solvent does not lie exactly on axis.

labeled A_α, A_β, A_γ, and B_α are 1,4-dioxane vibronic transitions which are built on A and B.

The 1,4-dioxane(Kr)₁ cluster and the 1,4-dioxane(Ar)₁ cluster have similar solvent physical properties and cluster spectroscopic properties. The spectrum of the 1,4-dioxane(Kr)₁ cluster is, therefore, interpreted in a fashion analogous to that for the 1,4-dioxane(Ar)₁ cluster. The binding energies of the 1,4-dioxane(Kr)₁ clusters are expected to be greater than those of the argon clusters due to the larger polarizability of Kr (Ar: $\alpha = 1.64 \text{ \AA}^3$; Kr: $\alpha = 2.48 \text{ \AA}^3$).¹⁹ A lower cluster binding energy for the argon cluster would account for the absence of features B_β and B_γ in the argon cluster spectrum.

B. 1,4-dioxane(methane)₁

The MRES of the 1,4-dioxane(CH₄)₁ and 1,4-dioxane(CD₄)₁ clusters are shown in Fig. 4. The negative peaks in these traces are due to ringing from the very intense bare molecule mass channel signal. Starting from the low energy end of the spectrum, a number of features are noteworthy: (i) a multiplet (labeled A), the lowest energy transition of which falls at 50 673.5 cm⁻¹, blue shifted 10.4 cm⁻¹ from the 1,4-dioxane origin, (ii) 64.1

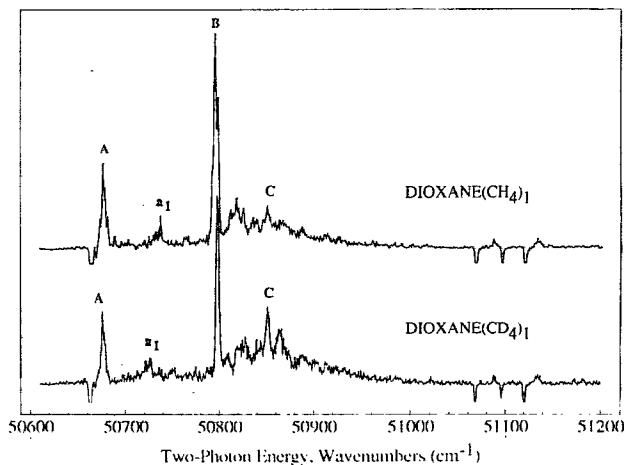


FIG. 4. Two photon one color (2+1) MRES of the 1,4-dioxane(CH₄)₁ cluster (top trace) and 1,4-dioxane(CD₄)₁ cluster (bottom trace).

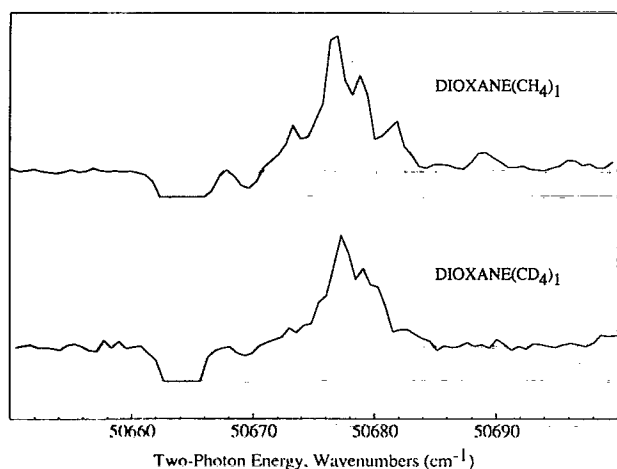


FIG. 5. Expanded view of Fig. 4 in the region of the cluster origin.

cm^{-1} from A is another less intense feature (labeled \mathbf{a}_1), (iii) a more intense feature (labeled B) which is resolved into two peaks, at $50\,795.8\text{ cm}^{-1}$ and $50\,798.7\text{ cm}^{-1}$, with a shoulder at $50\,792.8\text{ cm}^{-1}$, (iv) a broad and congested group of peaks (the largest peak of which is at $50\,851.4\text{ cm}^{-1}$ and labeled C), (v) a group of features at approximately $51\,095\text{ cm}^{-1}$, and (vi) no cluster signal is observed above $51\,200\text{ cm}^{-1}$.

The bottom trace of Fig. 4 shows how solvent deuteration affects the 1,4-dioxane(CH_4)₁ cluster spectrum. Three important effects should be noted: (i) the spacings in the initial multiplet (labeled A) collapse—this is shown in more detail in Fig. 5, (ii) the weak feature at $50\,737.6\text{ cm}^{-1}$ (labeled \mathbf{a}_1) is red shifted by 10.5 cm^{-1} to $50\,727.1\text{ cm}^{-1}$, (iii) the spacings between the resolved peaks in the most intense feature (labeled B) collapse from $2.9\text{--}1.3\text{ cm}^{-1}$.

Calculations produce three minimum energy geometries for the 1,4-dioxane(CH_4)₁ cluster as shown in Fig. 6. All three empirical methods of calculation (see Sec. II B) yield the same three geometries, but slightly different binding energies. As in the argon cluster case, the lowest energy configuration has the solvent molecule along the z axis of the defined coordinate system. Three methane hydrogen atoms point toward dioxane. The next lowest energy configuration is also analogous to the argon case with the methane carbon along the y axis. In the least stable geometry, three of the methane hydrogens point toward the C–C bond of the dioxane ring and the methane carbon is on the x axis. The resulting binding energies are listed in Table III and Fig. 6. The MOPAC 6 calculations produced only two different minimum energy geometries. In one of the MOPAC 6 geometries, methane is oriented in the y,z plane along a vector bisecting the y and z axes. The second MOPAC 6 geometry is equivalent to the least stable geometry determined by the empirical potential energy calculations. The resulting MOPAC 6 binding energies are also listed in Table III and are larger than any of the empirical potential results. These and the binding energies determined by the WERK program are probably too large considering that

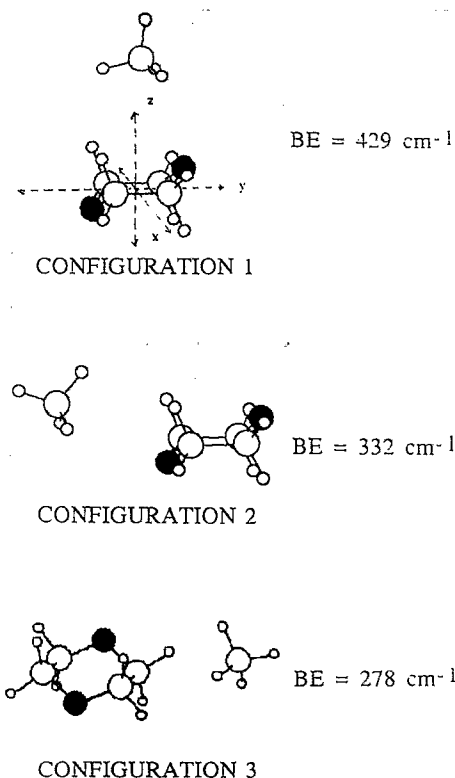


FIG. 6. Three minimum energy geometries of the 1,4-dioxane(CH_4)₁ cluster simulated with Scheraga's potential.

all cluster signal vanishes above 400 cm^{-1} to the blue of the bare 1,4-dioxane origin: an upper limit to the dioxane/methane ground state cluster binding energy is thus ca. 550 cm^{-1} . A cluster normal mode analysis is performed using the geometries determined by the Scheraga empirical potential. Identical geometries for deuterated methane are used to determine the effect of deuteration on these cluster van der Waals modes. The calculated frequencies for the van der Waals normal modes are listed in Table IV for the configurations calculated from the Scheraga potential.

The spectra in Fig. 4 are assigned based on empirical potential energy calculations and isotope shifts, in the following manner. The features labeled A, B, and C are assigned as spectral origins for three cluster configurations. The feature labeled \mathbf{a}_1 and the fine structure in A are assigned as van der Waals modes built on the origin of cluster A. The fine structure of B is likewise assigned as van der Waals modes of that cluster configuration. The assignment of the broad congested features labeled C is uncertain. The

TABLE III. Binding energies (cm^{-1}) for the three minimum energy 1,4-dioxane(CH_4)₁ and 1,4-dioxane(CD_4)₁ configurations.

Method	Configuration 1	Configuration 2	Configuration 3
Scheraga	429	332	278
WERK	666	534	480
MMX	439	396	320
MOPAC 6	900	900	404

TABLE IV. van der Waals normal mode frequencies (cm^{-1}) for three 1,4-dioxane(CH_4)₁ and three 1,4-dioxane(CD_4)₁ cluster geometries derived from the Scheraga potential energy form.

	Configuration ^a 1	Mode ^b type	Configuration 2	Mode type	Configuration 3	Mode type
1,4-dioxane(CH_4) ₁	84.2	T_y	69.8	T_x	71.9	T_y
	77.5	T_x	66.1	T_z	60.4	S_x
	72.3	S_x	65.5	S_y	56.0	T_z
	47.7	T_x	34.9	B_x	30.0	B_y
	37.3	B_y	21.8	T_y	26.7	T_x
	35.7	B_x	20.9	B_z	15.3	B_z
1,4-dioxane(CD_4) ₁	66.9	S_x	59.9	S_y	55.2	S_x
	60.7	T_y	49.4	T_x	51.2	T_y
	55.9	T_x	47.0	T_z	39.9	T_z
	39.3	B_x	31.3	B_x	28.8	B_y
	35.1	B_y	20.4	B_z	19.4	T_x
	29.5	T_x	16.8	T_y	14.8	B_z

^aFigure 6 illustrates the geometries of configurations 1–3 and the defined x, y , and z axis.

^bMode types stretch (S), torsion (T), and bend (B) have been defined in Ref. 21. The direction of motion indicated by the subscripts is approximate since the solvent does not lie exactly on axis.

calculations discussed above in this section suggest that this broad feature is due to a third cluster origin at $50\,851.4\text{ cm}^{-1}$ and van der Waals modes of the three cluster geometries. However, the possibility of C arising from multiple cluster geometries may not be ruled out. The observed van der Waals modes are most likely the totally symmetric modes for their respective cluster geometries based on the intensity of the allowed two photon spectrum and the observed Franck–Condon factors for the clusters and bare molecule. One is tempted to assign the most intense cluster origin to the most stable (largest binding energy) calculated cluster, but the van der Waals mode energies do not follow in this order for the totally symmetric species. Consequently, we do not suggest at present a relation between the observed cluster origin shifts and calculated cluster geometries.

Figure 5 shows the effect of deuteration on the origin A fine structure. The average spacings of 2.8 cm^{-1} for the partially resolved structure collapse in the deuterated species, suggesting that this progression is due to a very low frequency van der Waals mode. We suggest that the failure to model this intermolecular motion is due to the inability of the employed harmonic (force constant) calculation to model this low energy interaction. A similar type of phenomena is seen in the cluster configuration origin labeled B. Upon deuteration, the spacing between these two clearly resolved peaks is reduced from 3.0 cm^{-1} to 1.3 cm^{-1} and the shoulder at $50\,792.8\text{ cm}^{-1}$ disappears. This suggests that a similar type of motion also exists in this cluster conformation. The full spectrum for these clusters is tabulated and assigned in Table I.

C. 1,4-dioxane(CF_4)₁

Figure 7 displays the MRES of the 1,4-dioxane(CF_4)₁ cluster. Transition energies and their appropriate labels are listed in Table I. The spectral intensities above $51\,300\text{ cm}^{-1}$ in Fig. 7 have been multiplied by 2. The lowest energy transition (labeled A) is blue shifted

316.2 cm^{-1} from the bare 1,4-dioxane origin. A weaker feature appears 29.2 cm^{-1} further to the blue and is labeled a_1 . An intense feature (labeled B) appears at $51\,070.0\text{ cm}^{-1}$, blue shifted 406.9 cm^{-1} with respect to the dioxane 0_0^0 ; it has two partially resolved shoulder peaks to the high energy side at $51\,074.9\text{ cm}^{-1}$ and $51\,077.9\text{ cm}^{-1}$ (labeled b_1 and b_2). The transition labeled C appears at $51\,093.6\text{ cm}^{-1}$ and is blue shifted 430.6 cm^{-1} from the dioxane 0_0^0 . Appearing 414.0 cm^{-1} higher in energy than A is a weak feature A_α ; similarly, a feature labeled B_α is found 415.3 cm^{-1} to the blue of B, with two partially resolved shoulder features on the high energy side at $51\,490.3\text{ cm}^{-1}$ and $51\,494.5\text{ cm}^{-1}$ (labeled in Table I as $b_{\alpha 1}$ and $b_{\alpha 2}$, respectively). The feature labeled B_β at $51\,508.9\text{ cm}^{-1}$ is 438.9 cm^{-1} from B and the feature labeled B_γ at $51\,528.4\text{ cm}^{-1}$ is 458.4 cm^{-1} from B. No cluster transitions are detectable above $51\,600\text{ cm}^{-1}$. An experimental upper limit for the 1,4-dioxane(CF_4)₁ cluster binding en-

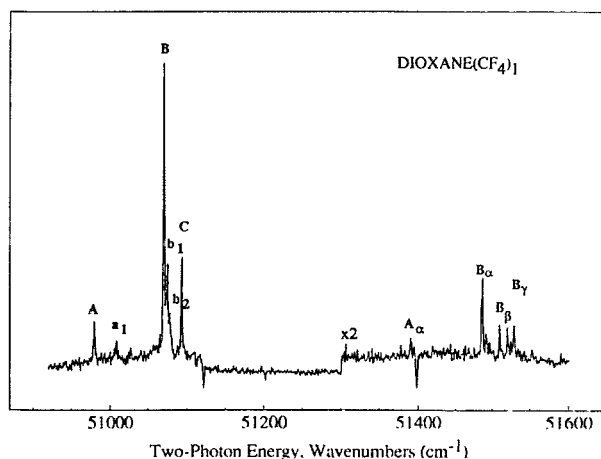


FIG. 7. Two photon one color (2+1) MRES of the 1,4-dioxane(CF_4)₁ cluster. For energies above $51\,300\text{ cm}^{-1}$, intensities have been increased by a factor of 2.

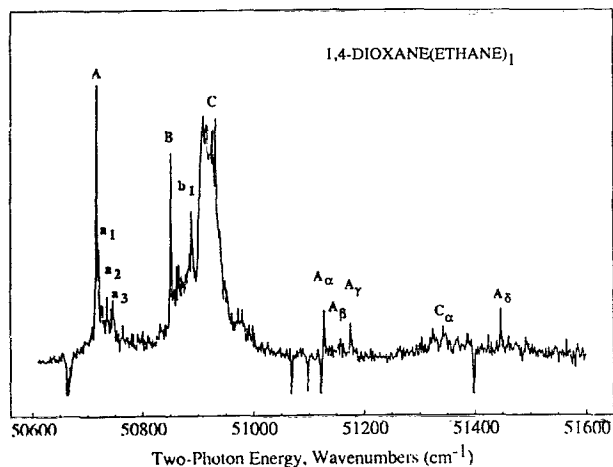


FIG. 8. Two photon one color (2+1) MRES of the 1,4-dioxane(ethane)₁ cluster.

ergy is approximately 600–700 cm^{-1} ; this is somewhat larger than that found for the 1,4-dioxane(CH_4)₁ cluster.

In light of the similarity between the CH_4 and CF_4 cluster spectra, the analysis of the spectrum displayed in Fig. 7 is analogous to that of the 1,4-dioxane(CH_4)₁ cluster spectrum. The feature labeled A is assigned as the spectral origin for one cluster geometry of dioxane(CF_4)₁. The feature labeled B is certainly an additional cluster geometry 0_0^0 transition. The weak feature labeled a_1 is assigned as a 29.2 cm^{-1} van der Waals mode built on A and the small peaks labeled b_1 and b_2 are most likely a 5 cm^{-1} van der Waals mode progression built on B. The feature labeled C is most likely a third cluster geometry origin. Due to their characteristic 410–415 cm^{-1} separation from their respective cluster origins, the features labeled A_α , B_α are assigned as the first 1,4-dioxane vibronic transition built on A and B. The feature labeled B_β is 438.9 cm^{-1} to the blue of B but is also 415.3 cm^{-1} to the blue of C. Therefore, B_β may be assigned as the second dioxane vibronic transition built on B, and the first dioxane vibronic transition built on C. A similar situation exists for B_γ , it being 458.4 cm^{-1} to the blue of B and 434.8 cm^{-1} to the blue of C and may therefore be assigned as the third and second dioxane vibronic transitions built on B or C, respectively. The peak between B_β and B_γ is a noise spike.

Calculations are not carried out for this system because good fluorine/carbon and fluorine/hydrogen potentials are not available in the various calculational algorithms.

D. 1,4-dioxane(ethane)₁

The MRES of the 1,4-dioxane(ethane)₁ cluster is displayed in Fig. 8. The lowest energy transition is observed at 50717.1 cm^{-1} (labeled A) and is blue shifted 54.0 cm^{-1} with respect to the 1,4-dioxane origin. There are three small peaks close to A (labeled a_1 , a_2 , and a_3) blue shifted with respect to A by 3.8, 18.3, and 29.6 cm^{-1} respectively. Shifted 188.3 cm^{-1} to the blue of the 1,4-dioxane origin is a sharp peak at 50851.4 cm^{-1} (labeled B) followed by another sharp peak at 50889.0 cm^{-1} (b_1) and a broad

intense feature, with some sharp structures, centered at 50907 cm^{-1} (labeled C). A group of three features (labeled A_α , A_β , and A_γ) is found at 51127.8 cm^{-1} , 51157.9 cm^{-1} , and 51175.1 cm^{-1} . A weak group of peaks is centered at ca. 51324 cm^{-1} (labeled C_α). Finally, a weak, sharp peak labeled A_δ is observed at 51446.9 cm^{-1} . The transition energies and relative energies for the 1,4-dioxane(ethane)₁ clusters are listed in Table I.

Force field calculations performed with Scheraga's empirical potential functions produce 22 different minimum energy geometries for the 1,4-dioxane(ethane)₁ cluster. These cluster conformations can be divided into three groups in which the ethane molecule lies approximately along one of the solute coordinate system axes defined in Sec. III A. For each of these groups, the ethane C–C bond axis may be oriented in many different ways with respect to the appropriate solute axis. Of the 22 calculated geometries, 10 have the ethane molecule oriented along the z axis with an average binding energy of 538(10) cm^{-1} , for 5 geometries the ethane molecule is oriented along the y axis with an average binding energy of 448(18) cm^{-1} , and in 7 geometries the ethane is oriented along the x axis with an average binding energy of 395(8) cm^{-1} . The reported number in parentheses is the average deviation of the energy in each grouping of structures. In each group a special conformation can be identified for which the ethane C–C bond axis is collinear to the defined solute axis. This is similar to the case of ethane clustered with benzene, for which calculations predict that ethane may bind with its C–C bond axis perpendicular or parallel to the plane of the ring, the most stable configuration being parallel to the ring plane.²⁰ When calculating the group mean values, the binding energies of the three cluster geometries in which the ethane C–C bond axis is collinear with the defined solute axes are not included. For this special case, the binding energies are 480, 374, and 307 cm^{-1} for the three groups described above, respectively. Nonetheless, the important result is that, within a particular representative group of structures the clusters along the z axis are most stable and those along the x axis are least stable. This is consistent with the results obtained for clusters in which the solvents are methane or argon. The experimentally determined upper limit for the 1,4-dioxane(ethane)₁ cluster binding energy is approximately 900 cm^{-1} (ca. feature A_δ). A normal mode analysis is performed on all of the 22 geometries to determine the magnitude of the van der Waals vibrational frequencies; the van der Waals modes for these geometries are between 10 cm^{-1} and 80 cm^{-1} .

In Fig. 8, the distinct peaks labeled A and A_α , A_β , A_γ , and A_δ are, respectively, assigned as the origin and dioxane vibronic transitions for one cluster conformation. These transitions are shifted approximately 55 cm^{-1} to the blue of the corresponding dioxane bare molecule transitions. Those peaks labeled a_1 , a_2 , and a_3 are assigned as van der Waals modes built on origin A. The peaks labeled B and b_1 are respectively assigned as the origin and van der Waals mode transitions of an additional cluster geometry. While the minimum energy geometry calculations do not provide a definitive interpretation of the spectrum, they do

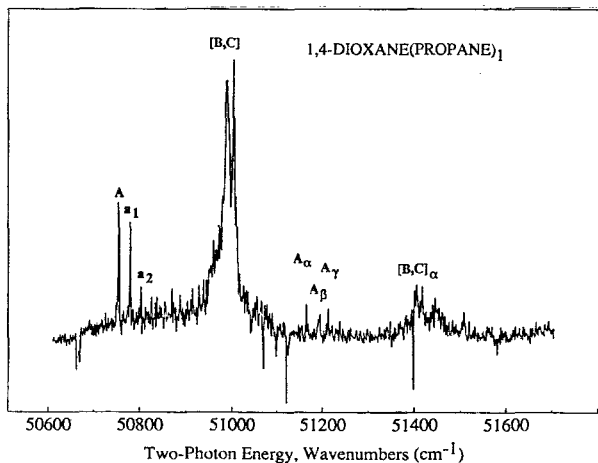


FIG. 9. Two photon one color (2+1) MRES of the 1,4-dioxane(propylene)₁ cluster.

support the proposal of multiple cluster geometries. Therefore, the features labeled C may be assigned as origins and/or van der Waals modes of a number of slightly different cluster geometries; however, note that the calculations predict multiple geometries for all three representative groups of cluster structures discussed above, while the spectrum suggests that only one of these groups displays such behavior.

E. 1,4-dioxane(propylene)₁

The MRES of the 1,4-dioxane(propylene)₁ cluster is displayed in Fig. 9. The lowest energy transition is at 50 756.4 cm⁻¹ (labeled A) and is blue shifted 93.3 cm⁻¹ with respect to the 1,4-dioxane bare molecule origin. Two peaks, labeled a₁ and a₂, are 24.6 cm⁻¹ and 48.8 cm⁻¹ to the blue of peak A. Two broad features (collectively labeled [B,C]) are located at 50 988.8 cm⁻¹ and 51 004.0 cm⁻¹. The first of a group of three peaks (labeled A_α, A_β, and A_γ) appears at 51 165.9 cm⁻¹. Centered at 51 407 cm⁻¹ is a group of broad features labeled [B,C]_α. The transition energies for the 1,4-dioxane(propylene)₁ cluster are listed in Table I.

Empirical potential energy calculations produce 65 minimum energy geometries for the 1,4-dioxane(propylene)₁ cluster. These geometries may also be divided into three groups in the same manner described above for the 1,4-dioxane(ethane)₁ cluster; however, this categorization is now complicated by the additional complexity of the solvent propane introducing a number of subcategories. The details of all of these subcategories are not instructive: in all cases of equivalent orientation of the propane along a given solute coordinate system axis, the geometries with propane along the z axis are most stable and those along the x axis are least stable with binding energies ranging from 400–700 cm⁻¹. The experimentally determined upper limit for the 1,4-dioxane(propylene)₁ cluster binding energy is approximately 900–1000 cm⁻¹. A normal mode analysis of these geometries produces van der Waals mode energies between 10 cm⁻¹ and 65 cm⁻¹.

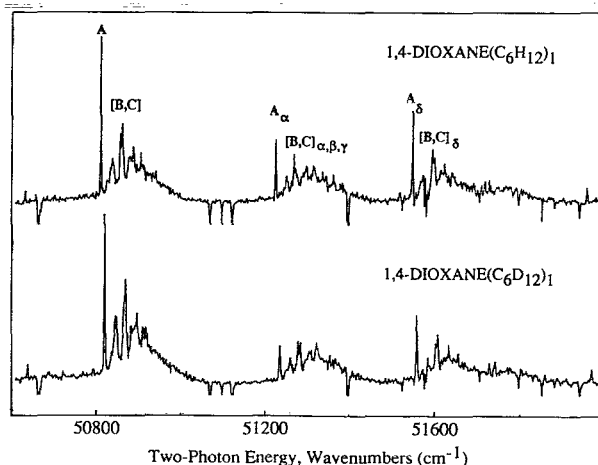


FIG. 10. Two photon one color (2+1) MRES of the 1,4-dioxane(cyclohexane-*h*₁₂)₁ cluster (top trace) and the 1,4-dioxane(cyclohexane-*d*₁₂)₁ cluster (bottom trace).

The detailed assignments for the observed features for this cluster system are based on those for dioxane (CH₄)₁, (CF₄)₁, and (C₂H₆)₁; these are given in Table I. The difference is that, in the dioxane(propylene)₁ cluster spectrum, one cannot distinguish between the B and C cluster origins due to the apparent similarity of their transition energies.

F. 1,4-dioxane(cyclohexane)₁

Figure 10 displays the MRES of 1,4-dioxane(cyclohexane-*h*₁₂)₁ (top trace) and 1,4-dioxane(cyclohexane-*d*₁₂)₁ (bottom trace). The positions of the dioxane origin and vibronic transitions appear in these spectra as negative signals. The top trace shows three groups of features, the lowest energy peak in each group is labeled A, A_α, and A_δ. The energies of the first three transitions in each group are listed in Table I. Each of these groups has a sharp feature at the low energy side and followed by a number of broad features spanning approximately 100 cm⁻¹. The bottom trace in Fig. 10 shows that upon deuteration of cyclohexane the positions of all of these features are shifted approximately 10 cm⁻¹ to the blue, but the relative spacings between these features do not change.

Potential energy calculations for the 1,4-dioxane(cyclohexane)₁ cluster produce 50 minimum energy configurations. Due to the relatively large size of the solvent molecule and the similarity of the solute and solvent, these geometries cannot be categorized in the manner stated above for the smaller solvents. The binding energies for these geometries range from 450–890 cm⁻¹. The experimental upper limit for the 1,4-dioxane(cyclohexane)₁ cluster binding energy is approximately 1100–1300 cm⁻¹. A normal mode analysis of these geometries produces van der Waals mode frequencies between 8 cm⁻¹ and 65 cm⁻¹. Upon deuteration of cyclohexane, these calculations predict a 0.5–4 cm⁻¹ decrease in van der Waals mode frequencies.

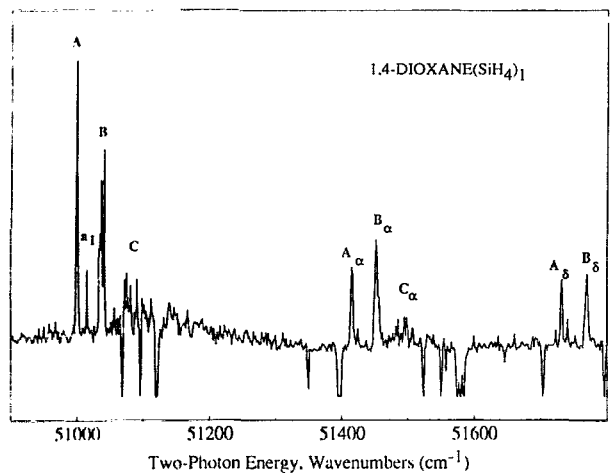


FIG. 11. Two photon one color (2+1) MRES of the 1,4-dioxane (SiH_4)₁ cluster.

Based on the minimum energy geometry calculations and the normal mode analysis, the feature labeled **A** are assigned as the spectral origin for one cluster geometry and the group of features labeled **[B,C]** are assigned as the spectral origins of multiple cluster configurations. If these broad, congested features were van der Waals vibrational modes, one would expect a reduction in their relative energies upon deuteration; however, no significant reduction of these differences is observed. The peaks labeled A_α and the first two peaks in the group labeled $[B,C]_{\alpha,\beta,\gamma}$ are shifted approximately 414 cm^{-1} from origins **A** and $[B,C]$, respectively, and this corresponds to the first 1,4-dioxane vibronic transition. Likewise, the peaks labeled A_δ and $[B,C]_\delta$ are shifted approximately 737 cm^{-1} from those labeled **A** and $[B,C]$, respectively; this spacing corresponds to the fourth observed 1,4-dioxane vibronic transition. The transition energies, relative energies, and assignments are listed in Table I.

G. 1,4-dioxane(SiH_4)₁

A trace of the 1,4-dioxane(SiH_4)₁ cluster MRES is shown in Fig. 11. The analysis of this spectrum is analogous to that of 1,4-dioxane(CH_4)₁. The first peak which appears at $50\,999.9\text{ cm}^{-1}$ is blue shifted by 336.8 cm^{-1} with respect to the bare 1,4-dioxane origin. This peak is assigned as the origin of one cluster configuration and is labeled **A**. A small sharp peak blue shifted 14.9 cm^{-1} with respect to **A** is assigned as a van der Waals mode built on **A**. The three peaks (grouped close together and labeled **B**) may be assigned as either origins of slightly different cluster geometries and/or van der Waals modes; however, their intensity pattern suggests that they are the result of different cluster geometries. To higher energy a group of features labeled **C** is centered at approximately $51\,075\text{ cm}^{-1}$. The presence of many features in this group may be attributed to either multiple cluster geometries, van der Waals vibrational modes, or a combination of both. The features labeled A_α , B_α , and C_α are assigned as the dioxane 415 cm^{-1} vibronic transition built on **A**, **B**, and **C**, respec-

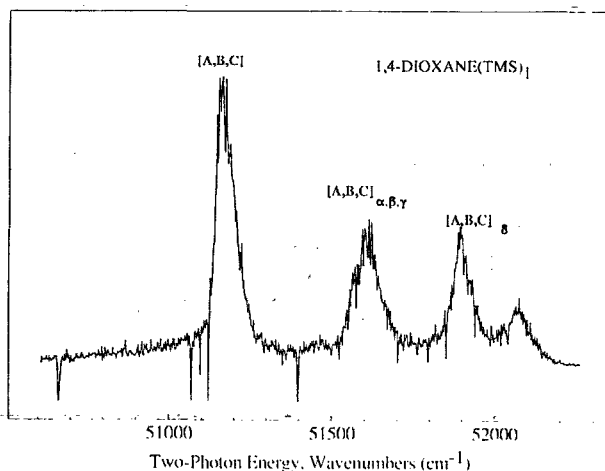


FIG. 12. Two photon one color (2+1) MRES of the 1,4-dioxane (TMS)₁ cluster.

tively. Likewise, the features labeled A_γ and B_γ are assigned as the dioxane 734 cm^{-1} vibronic transition built on **A** and **B**. No cluster signal is observed above $51\,800\text{ cm}^{-1}$. This suggests an upper limit to the cluster binding energy of $1100\text{--}1200\text{ cm}^{-1}$. This result seems high in light of the results for the 1,4-dioxane(methane)₁ and 1,4-dioxane(CF_4)₁ clusters.

H. 1,4-dioxane(TMS)₁

The MRES of the 1,4-dioxane(tetramethylsilane- TMS)₁ cluster is shown in Fig. 12. The spectrum consists of four broad features, the first three of which are labeled $[A,B,C]$, $[A,B,C]_{\alpha,\beta,\gamma}$, and $[A,B,C]_\delta$. The low energy edge of $[A,B,C]$ is blue shifted 475 cm^{-1} with respect to the 1,4-dioxane origin. The low energy edge of $[A,B,C]_{\alpha,\beta,\gamma}$ and $[A,B,C]_\delta$ are approximately 410 cm^{-1} and 730 cm^{-1} from **A**, respectively. The full width at half-height of $[A,B,C]$, $[A,B,C]_{\alpha,\beta,\gamma}$, and $[A,B,C]_\delta$ are approximately 60, 95, and 60 cm^{-1} , respectively. The transition energies and the half-height widths of these features suggest that $[A,B,C]$ is the origin transition for many clusters, $[A,B,C]_{\alpha,\beta,\gamma}$ corresponds to the first three 1,4-dioxane vibronic transitions, and $[A,B,C]_\delta$ corresponds to the fourth 1,4-dioxane vibronic transition. The breadth of these features is a result of multiple geometries and/or low frequency van der Waals modes. Although TMS is similar to methane, tetrafluoromethane, and silane (specifically, they are all symmetric top molecules), the 1,4-dioxane(TMS)₁ cluster spectrum is very similar to that of cyclohexane. No signal is observed above $52\,200\text{ cm}^{-1}$. This suggests an upper limit to the cluster binding energy of 2000 cm^{-1} . This binding energy is quite high in light of other cluster results. This result most likely represents the inability of large amounts of energy to find its way into the reaction coordinate for dissociation due to a high density of states.

IV. CONCLUSIONS

One color 2+1 mass resolved excitation spectroscopy is used to obtain molecular Rydberg spectra of 1,4-dioxane clustered with nine nonpolar solvents. These spectra are analyzed in terms of calculations which model the minimum energy cluster geometry and the van der Waals normal mode energies for these structures. The results show that, as the solvent becomes more complex, so do the cluster spectra and calculated cluster structures. For 1,4-dioxane clustered with Ar and Kr, model calculations indicate that two cluster geometries exist: this is in good agreement with spectral results. Comparable results are obtained by a similar analysis of the 1,4-dioxane(methane)₁ cluster spectra. In this case, computer simulations find three stable cluster geometries, two of which have analogous structures and binding energies to those found for dioxane clustered with Ar and Kr, and a third which is less stable. These assignments are also confirmed by the deuteration (and fluorination) of methane which facilitates the discrimination of transitions resulting from either van der Waals modes or different cluster geometries. These results show that, for this system, empirical potential energy calculations provide a reasonable model for cluster geometries and intermolecular van der Waals modes. An exception to this generalization is the apparent inability of the employed harmonic potential to model very low frequency intermolecular motions such as those observed for the 1,4-dioxane(methane)₁ cluster spectrum. For 1,4-dioxane clustered with ethane, broad features appear in the spectrum which are assigned as a combination of multiple cluster geometries and van der Waals modes based on the cluster geometry simulations and the magnitude of the calculated van der Waals normal mode energies. This trend continues, with the cluster Rydberg spectra becoming more congested for dioxane clustered with propane, silane, tetramethylsilane (TMS), and cyclohexane. This is most likely due to two things which are a result of increasing solvent complexity: (i) the number of possible cluster geometries increases, and (ii) the difference in transition energies for these geometries decreases.

An upper limit for the cluster binding energy may be determined from the energy at which the cluster signal vanishes. These maximum binding energies are approximately 100–300 cm⁻¹ greater than calculated binding energies. This difference probably reflects the relative efficiency at which a sufficient amount of excess vibrational energy may relax into the reaction coordinate for intermolecular dissociation (i.e., the rates of intracuster vibrational redistribution and vibrational predissociation).

For all of the clusters, the electronic origins are blue

shifted with respect to the bare 1,4-dioxane origin. The spectral shift for a cluster can be viewed as the difference between the ground and excited state binding energies. Therefore, the observed blue shift indicates that the cluster is destabilized upon excitation to its molecular Rydberg state. This observation is consistent with the model in which the excited state intermolecular potential becomes repulsive due to the increased radial distribution of the excited electron in the Rydberg state.

ACKNOWLEDGMENT

This work was supported in part by a grant from ARO.

- ¹(a) M. B. Robin, *Higher Excited States of Polyatomic Molecules*, Vol. I (Academic, New York, 1974); (b) M. B. Robin, *Higher Excited States of Polyatomic Molecules*, Vol. II (Academic, New York, 1975).
- ²(a) T. J. Cornish, and T. Baer, *J. Am. Chem. Soc.* **109**, 6915 (1987); (b) T. J. Cornish, and T. Baer, *ibid.* **110**, 3099 (1988); (c) T. J. Cornish, and T. Baer, *J. Phys. Chem.* **94**, 2852 (1990).
- ³T. J. Cornish, T. Baer, and L. G. Pedersen, *J. Phys. Chem.* **93**, 6064 (1989).
- ⁴(a) R. L. Whetten, K. J. Fu, and E. R. Grant, *J. Chem. Phys.* **79**, 2626 (1983); (b) S. G. Grubb, R. L. Whetten, A. C. Albrecht, and E. R. Grant, *Chem. Phys. Lett.* **108**, 420 (1984); (c) R. L. Whetten, S. G. Grubb, C. E. Otis, A. C. Albrecht, and E. R. Grant, *J. Chem. Phys.* **82**, 1115 (1985); (d) S. G. Grubb, C. E. Otis, R. L. Whetten, E. R. Grant, and A. C. Albrecht, *J. Chem. Phys.* **82**, 1135 (1985).
- ⁵R. L. Whetten, K. J. Fu, and E. R. Grant, *Chem. Phys.* **90**, 155 (1984).
- ⁶(a) R. L. Whetten, and E. R. Grant, *J. Chem. Phys.* **81**, 691 (1984); (b) R. L. Whetten, K. S. Haber, and E. R. Grant, *J. Chem. Phys.* **84**, 1270 (1986).
- ⁷R. L. Whetten, and E. R. Grant, *J. Chem. Phys.* **80**, 1711 (1984).
- ⁸*Atomic and Molecular Clusters*, edited by E. R. Bernstein (Elsevier, New York, 1990).
- ⁹D. J. Donaldson, G. A. Gaines, and V. Vaida, *J. Phys. Chem.* **92**, 2766 (1988).
- ¹⁰D. J. Donaldson, E. C. Richard, S. J. Strickler, and V. Vaida, *J. Phys. Chem.* **92**, 5514 (1988).
- ¹¹D. J. Donaldson, R. Naaman, and V. Vaida, *J. Phys. Chem.* **87**, 2522 (1987).
- ¹²S. H. Lin, Y. Fujimura, H. J. Neusser, E. W. Schlag, *Multiphoton Spectroscopy of Molecules* (Academic, New York, 1984).
- ¹³E. R. Bernstein, K. Law, and M. Schauer, *J. Chem. Phys.* **80**, 207 (1984).
- ¹⁴(a) G. Nemethy, M. S. Pottle, and H. A. Scheraga, *J. Phys. Chem.* **87**, 1883 (1983). (b) J. F. Yan, F. A. Momany, R. Hoffmann, and H. A. Scheraga, *J. Phys. Chem.* **74**, 420 (1970). (c) F. A. Momany, R. F. McGuire, J. F. Yan, H. A. Scheraga, *J. Phys. Chem.* **74**, 2424 (1970). (d) R. F. McGuire, F. A. Momany, and H. A. Scheraga, *J. Phys. Chem.* **76**, 375 (1972).
- ¹⁵J. J. P. Stewart, *A General Molecular Orbital Package MOPAC*, 6th ed.
- ¹⁶A. K. Rappé, C. J. Casewit, K. S. Colwell, W. A. Goddard III, and W. M. Skiff, preprint.
- ¹⁷*Molecular Modeling Software for the IBM/AT*, 4th ed., Serena, 1990.
- ¹⁸S. Li, and E. R. Bernstein, *J. Chem. Phys.* **95**, 1577 (1991).
- ¹⁹T. M. Miller, and B. Bederson, *Adv. At. Mol. Phys.* **13**, 1 (1977).
- ²⁰M. Schauer, and E. R. Bernstein, *J. Chem. Phys.* **82**, 726 (1985).